Large Eddy Simulation of Multi-Component Mixing Layers at High-Pressure Conditions

Kuetemeier*[1], Ries[1], Sadiki[1]
[1]Technische Universität Darmstadt, Energy and Power Plant Technology, Darmstadt, Germany
*Corresponding author: kuetemeier@ekt.tu-darmstadt.de

Abstract
There is a growing interest in processes of trans- and supercritical atomization in high pressure and temperature applications, e.g. rocket engines, high pressure piston engines, chemical production, etc.. Therefore a detailed understanding of trans- and supercritical processes is essential to improve such applications. Those applications have an injection process in common. Thereby sub- or supercritical single as well as multi-component fluids are injected, atomized and/or mixed. To support jet injection design tasks, numerical simulations are necessary. To deal with usually involved complex configurations and geometries, it is well accepted to decrease the complexities while keeping the essential features of the application under consideration. In this contribution a mixing layer which includes a shear layer boundary to mimic the interface of separated fluids is studied. Thereby, complex species diffusion and mixing processes take place.
Despite the increased available computational power, direct numerical simulations (DNS) of such high pressure mixing processes are not efficiently feasible. In order to establish a numerical tool which is computationally efficient and economically acceptable, the present contribution suggests a Large Eddy Simulation (LES) framework which includes the Smagorisky subgrid-scale model and well adapted multi-component species diffusion and mixing models to study the Okong'o configuration. In this configuration two fluids, composed of pure oxygen and hydrogen, respectively, are forced under supercritical conditions to build a predefined binary shear layer with temporal vortex roll ups in order to explore the features of the interface mixing with initial density stratifications up to 24.4.
All LES simulations are conducted with the open-source solver OpenFOAM utilizing an in-house low Mach solver which includes real gas properties by means of the Peng-Robinson equation of state to deal with high pressure conditions.
Global shear layer mixing features are examined over time to describe the mixing. Developing vortices leading to specific temporal enstrophy and vorticity are compared to reference DNS data, especially the mixing processes within the temporal vortex roll ups, in order to validate the utilized diffusion and mixing models.

Keywords
LES, supercritical, multi-component mixing, shear layer

Introduction

Modern energy conversion applications are increasingly operating under trans- or supercritical conditions. This mainly results from demands for higher combustion efficiencies and less noxious energy conversions. Especially in liquid rocket engines (LRE) high level pressures are desired to maximize the available payloads. In such applications fuels and oxidizers are typically injected at high pressures and temperatures. Until today high-pressure injections of super- or transcritical fluids injected into supercritical environments are not completely comprehended. During the last decades a few research groups focused on supercritical phenomena. Especially shadowgraphic studies were rolled out in the early days of trans- and supercritical jet injection investigations. Cheroudi et al. [1] performed trans- and supercritical jet injections of nitrogen into nitrogen. Fine ligaments of fluid were investigated in supercritical areas of the observed supercritical jets in contrast to subcritcal injection where formations of droplets take place. This effect is due to the diminishing surface tension when fluids cross or exceed the critical values of pressure and temperature. In consequence the formation of droplets is suppressed. In supercritical conditions the effects of surface tension are subordinate and thermodynamic, as well as turbulent mechanisms become predominant in the jet interface area resulting into finger like structures on the fluid interface.
Similar fluid mixing behaviour can be observed in multicomponent mixtures. Especially, Mayer et al. [2] investigated co-axial injections of liquid nitrogen into gaseous helium with a gaseous co-flow. If the pressure of the chamber is exceeding the critical temperature of the mixture, fluid like phenomena can be observed. The subcritical formation of jet breakup into small droplets becomes replaced by a frayed finger like interface, where surface tension is playing a minor role. Roy et al. [3] investigated similar mixture injections of nitrogen jets, confirmed this overall behavior. Due to the main application of supercritical combustion in LREs, many studies target on conditions adjusted for turbulent jets resulting in large Reynolds numbers. Therefore a great computational effort needs to be applied in order to archive representative results of supercritical jet injections.
If a fluid is injected into a chamber filled with more or less quiescent fluid, one can expect the same effects to take place like in a shear layer. Attending to that, Kawai [4] investigated transcritical boundary layers, were related phenomena of turbulent vortex developments take place.
Miller et al. [5] were the first who conducted direct numerical simulations (DNS) of various supercritical shear layer

This work is licensed under a Creative Commons 4.0 International License (CC BY-NC-ND 4.0).

configurations. Thus these DNS results are predestined to investigate numerical models of supercritical mixtures and their interfaces. Two initially separated layers of hydrogen and oxygen will interact with each other and develop a fully turbulent shear layer by artificial embossed periodic momentum. The present study will focus on the interface area of jets by abstracting them into a shear layer computation, based on the DNS results by Okong'o et al [6]. Large Eddy Simulation (LES) technique, known for its computational affordability in comparison to DNS is used as it is capable of capturing the large turbulent structures, while the small sub-grid-scales (SGS) are modeled. To account for the non-ideal fluid at supercritical conditions, the commonly applied Peng-Robinson equation of state (PR-EOS) including mixing rules will be used [7].
In addition Ries et al. [8] introduced a new low-Mach approach. This was first tested on a numerical single-species configuration based on the experiments by Mayer et al. [2], but with moderate Reynolds number. Recently, further tests of the low-Mach approach were conducted with single-species annulus configurations, see [9]. The present study is conducted to test and stretch the known borders of the 2. order stability of the utilized low-Mach approach, by investigating the vorticity and enstrophy of the developing turbulent structures in the shear layer configuration.
The paper is organized as following: Section 2 introduces the methods alongside the modeling approaches. Section 3 describes the test case and the numerical setup. In Section 4 the results are presented and discussed. Section 5 is devoted to conclusion.

Methods
A Large Eddy Simulation (LES) with an incompressible low-Mach solver is utilized in this study, in accordance to Ries et al. [8] and Müller et al. [10] .
The following system of governing filtered equations is solved for:

$$\frac{\partial \bar{\rho}}{\partial t} + \frac{\partial}{\partial x_j}\left(\bar{\rho}\tilde{u}_j\right) = 0 \tag{1}$$

$$\frac{\partial \bar{\rho}\tilde{u}_j}{\partial t} + \frac{\partial}{\partial x_j}\left(\bar{\rho}\tilde{u}_i\tilde{u}_j\right) = -\frac{\partial \bar{p}}{\partial x_j} + \frac{\partial}{\partial x_j}\left(\bar{\tau}_{ij} - \bar{\rho}\tau_{ij}^{SGS}\right) \tag{2}$$

$$\frac{\partial \bar{\rho}Y_O}{\partial t} + \frac{\partial}{\partial x_j}\left(\bar{\rho}Y_O\tilde{u}_j\right) = -\frac{\partial}{\partial x_j}\left(j_{O,j} + \bar{\rho}j_{O,j}^{SGS}\right) \tag{3}$$

$$\frac{\partial \bar{\rho}\tilde{h}}{\partial t} + \frac{\partial}{\partial x_j}\left(\bar{\rho}\tilde{u}_j\tilde{h}\right) = -\frac{\partial}{\partial x_j}\left(q_j + \bar{\rho}q_j^{SGS}\right) \tag{4}$$

Where t is time, $\bar{\rho}$ the density, $\tilde{u}_i$ the velocity, $\bar{p}$ the modified thermodynamic pressure, $\tilde{h}$ the enthalpy and Y_O the mass fraction of O2. Filtered variables are described by $\tilde{}$, while ^{SGS} represents sub-grid-scale quantities. On right hand side of the equations appear several flux vectors: molecular and sub-grid-scale-heat flux q_j, q_j^{SGS} as well as mmolecular and sub-grid-scale mass flux of oxygen $j_{O,j}$, $j_{O,j}^{SGS}$. Because of the binary system only the equation for one species (oxygen) is solved, see eqn. (3). The hydrogen mass fraction deviation is calculated by solving: $Y_H = 1 - Y_O$. In addition the Newtonian viscous stress tensor and sub-grid-scale stress tensor is modeled as:

$$\tau_{ij} = -\nu\left(\frac{\partial \tilde{u}_i}{\partial x_j} + \frac{\partial \tilde{u}_j}{\partial x_i} - \frac{2}{3}\frac{\partial \tilde{u}_k}{\partial x_k}\delta_{ij}\right); \qquad \tau_{ij}^{SGS} = -\nu^{SGS}\left(\frac{\partial \tilde{u}_i}{\partial x_j} + \frac{\partial \tilde{u}_j}{\partial x_i} - \frac{2}{3}\frac{\partial \tilde{u}_k}{\partial x_k}\delta_{ij}\right) \tag{5}$$

Where δ_{ij} is the Kronecker-delta function and ν^{SGS} is the sub-grid-scale kinematic viscosity introduced by the Smagorinsky sub-grid approach used. The viscosity ν is determined by means of the correlations of Chung et al. [11]
The flux vectors are modeled as:

$$j_{O,j} = -\left[j'_{O,j} + \left(\alpha_{IK} - \alpha_h\right)Y_O Y_H \frac{\bar{\rho}D}{T}\frac{\partial T}{\partial x_j}\right]; \qquad j_{O,j}^{SGS} = -\frac{\nu^{SGS}}{Sc^{SGS}}\frac{\partial Y_O}{\partial x_j} \tag{6}$$

Where α_{IK} and α_h are transport coefficients associated to molar and heat fluxes. The diffusion factor D is derived from $Sc = \nu\alpha_D D$, with mass diffusion factor α_D and:

$$j'_{O,j} = \bar{\rho}D\left[\alpha_D\frac{\partial Y_O}{\partial x_j} + \frac{Y_O Y_H}{RT}\frac{m_O m_H}{m}\left(\frac{v_O}{m_O} - \frac{v_H}{m_H}\right)\frac{\partial p}{\partial x_j}\right] \tag{7}$$

Where m_β are the molar masses of species β and m is the molar mass of the mixture, while v_β are the partial molar volumes of species β, with $v_\beta = (\partial v/\partial X_\beta)$. Where X_β is the molar fraction of species β ($X_\beta = mY_\beta/m_\beta$) and R is

This work is licensed under a Creative Commons 4.0 International License (CC BY-NC-ND 4.0).

the universal gas constant. But because of the low-Mach solver approach, $\partial p/\partial x_j$ tends to zero. Furthermore the heat flux vector is modeled as:

$$q_j = -\lambda \frac{\partial T}{\partial x_j} - \alpha_{IK} R T \frac{m}{m_O m_H} j'_{O,j}; \qquad q_j^{SGS} = -\frac{\nu^{SGS}}{Pr^{SGS}} \frac{\partial \tilde{h}}{\partial x_j} \tag{8}$$

With thermal conductivity λ. Where Sc^{SGS} is the sub-grid-scale Schmidt number and Pr^{SGS} is the sub-grid-scale Prandtl number. To account for the real gas effects, the Peng-Robinson equation of state is applied:

$$p = \frac{RT}{\tilde{v} - b_m} - \frac{(\alpha a)_m}{\tilde{v}^2 + 2b\tilde{v} - b^2} \tag{9}$$

with

$$\alpha = \left[1 + \left(0.37464 + 1.54226\kappa - 0.26992\kappa^2\right)\left(1 - \sqrt{\frac{T}{T_c}}\right)\right] \tag{10}$$

$$a = 0.45724 \frac{(RT_c)^2}{P_c} \tag{11}$$

$$b = 0.0778 \frac{RT_c}{P_c} \tag{12}$$

Where T_c is the critical Temperature and P_c the critical pressure.
The parameters $(\alpha a)_m$ and b_m are defined by means of the Peng-Robinson mixing rules:

$$(\alpha a)_m = \sum_i \sum_j X_i X_j (\alpha a)_{ij} \quad \text{where} \quad (\alpha a)_{ij} = \sqrt{(\alpha a)_i (\alpha a)_j}\,(1 - k_{ij}) \quad \text{and} \quad b_m = \sum_i X_i b_i \tag{13}$$

The whole framework was implemented in the OpenSource computational fluid dynamics software OpenFOAM Version 4.0 to solve the following test case.

Test case
The analyzed case is that investigated by Okong'o et al. [6] by means of DNS. In this case a supercritical binary species system consisting of oxygen and hydrogen is forced to develop particular stationary vortex roll-ups. This is achieved by a specific initial solution taking into account the development of the initiated vorticity structures.
The computational domain is spanned $L_1 = 0.2m$ in streamwise direction x_1, $L_2 = 0.2m$ in spanwise direction x_2 and $0.12m$ in crossstream direction x_3. However, due to the large pressure fluctuations in crosstream direction, additional buffer layers were introduced in this direction increasing the crossstream expansion to $L_3 = 0.6m$:

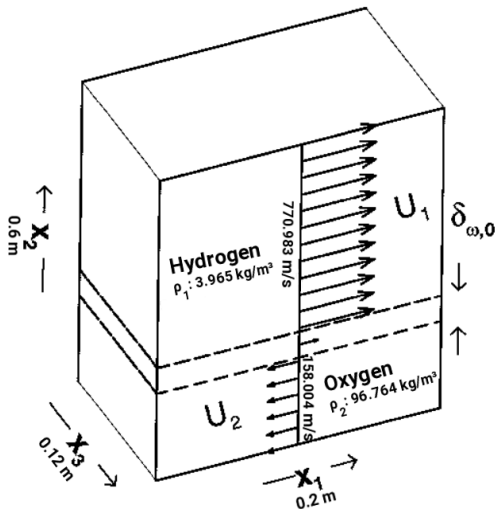

Figure 1. Computational domain according to Okong'o et al. [6]

This work is licensed under a Creative Commons 4.0 International License (CC BY-NC-ND 4.0).

Table 1. Mean flow properties and critical properties

Quantity	Oxygen	Hydrogen
$\bar{u}$ in m/s	-158.004	770.983
$\bar{\rho}$ in kg/m^3	69.764	3.965
p in N/m^2	$10.13 \cdot 10^6$	$10.13 \cdot 10^6$
T in K	400	600
T_c in K	154.58	33
m in kg/mol	$2.0159 \cdot 10^{-3}$	$31.9988 \cdot 10^{-3}$
P_c in N/m^2	$1.2838 \cdot 10^6$	$5.043 \cdot 10^6$

Figure 1 is also depicting the main velocity distribution in streamwise direction. In the upper hydrogen filled volume the mean velocity is pointing streamwise, while in the oxygen volume the mean velocity is pointing in counter streamwise direction. Those mean velocity profiles are merged into each other by a error function, as well as the temperature and density distributions, see table 1.
Hence the case has a initial density stratification of 24.4.
The two species (oxygen / hydrogen) are separated at the beginning and will initiate a mixing process enforced by the initial momentum conditions. Thereby a shear layer with specific properties develops, resulting in a set of stationary vortex structures, finally combining to one vortex. The initial velocity contribution is designed to keep the vortex in a stationary position.
The utilized low-Mach solver is working in the framework of OpenFOAM calculating velocity fields, in contrast to the DNS approach by Okong'o et al [6], where vorticity fileds are solved. Therefore in this study a initial velocity field was derived from the given vorticity profiles, by solving a Poisson equation. In consequence this approach leads to a velocity field specific wave structure in streamwise and spannwise directions, superimposed on the initial mean velocity field. The streamwise and spanwise initial vorticity perturbations are given by:

$$\omega_1\left(x_2, x_3\right) = F_{3D} \frac{\lambda_1 \Delta U_0}{\Gamma_1} f_2\left(x_2\right) f_3\left(x_3\right) \tag{14}$$

The spanwise vorticity perturbation factors are given by: $F_{3D} = 0.05$, $B_0 = 1$, $B_1 = 0.025$.

$$\omega_3\left(x_1, x_2\right) = F_{2D} \frac{\lambda_3 \Delta U_0}{\Gamma_3} f_1\left(x_1\right) f_2\left(x_2\right) \tag{15}$$

The streamwise vorticity perturbation factors are given by: $F_{2D} = 0.1$, $A_0 = 1$, $A_1 = 0.5$, $A_2 = 0.35$, $A_3 = 0.35$.
Furthermore the initial vorticity functions are derived from:

$$f_1\left(x_1\right) = A_0 \left|sin\left(\frac{\pi x_1}{\lambda_1}\right)\right| + A_1 \left|sin\left(\frac{\pi x_1}{2\lambda_1}\right)\right| + A_2 \left|sin\left(\frac{\pi x_1}{4\lambda_1}\right)\right| + A_3 \left|sin\left(\frac{\pi x_1}{8\lambda_1} - \frac{\pi}{2}\right)\right| \tag{16}$$

$$f_2\left(x_2\right) = exp\left[-\pi\left(\frac{x_2}{\delta_{\omega,0}}\right)^2\right] \tag{17}$$

$$f_3\left(x_3\right) = B_0 \cdot sin\left(\frac{2\pi x_3}{\lambda_3}\right) + B_1 \cdot sin\left(\frac{\pi x_3}{L_3}\right) \tag{18}$$

The initial vorticity thickness $\delta_{\omega,0} = 6.859 * 10^{-3}$ and the wavelengths $\lambda_1 = 7.29\delta_{\omega,0}$, $\lambda_3 = 0.6\lambda_1$ represent the most unstable incompressible wavelengths. These are the dominant wavelength in the deployment of the stationary vortices.

It turns out that the quality of the initial solution obtained by the transformation of initial vorticity functions into velocity data is depending on the mesh resolution. Therefore the initial solution was calculated on a similar grid as the reference DNS data, consisting of 532 x 532 x 208 cells in the core domain plus additional cells in the buffer regions, resulting in 29 million cells. The resulting velocities fields are then transferred onto smaller meshes consisting of 88 x 88 x 52 for LES calculations, which results in 549120 cells in the core region and 549120 cells including the buffer layers.
Periodic boundaries in streamwise and spannwise directions represent a infinitely spatial expansion of the free shear layer. In crossstream direction, a mixed boundary condition is applied. This boundary condition calculates

This work is licensed under a Creative Commons 4.0 International License (CC BY-NC-ND 4.0).

the total pressure based on the velocity and determines whether a Neumann- or Dirichlet boundary condition is applied for the velocity field based on the flux direction. A second order central differencing scheme is utilized for the convection terms and a second order, conservative scheme for the Laplacian terms. Second order backward integration method is utilized for the time derivative terms.

Results

Figure 2 shows a comparison of LES data (left) versus reference data (right) of the nondimensional spanwise vorticity in the braid plane at $x_3 = 0.0075$ and $t\Delta U_0/\delta_{\omega,0} = 80$.

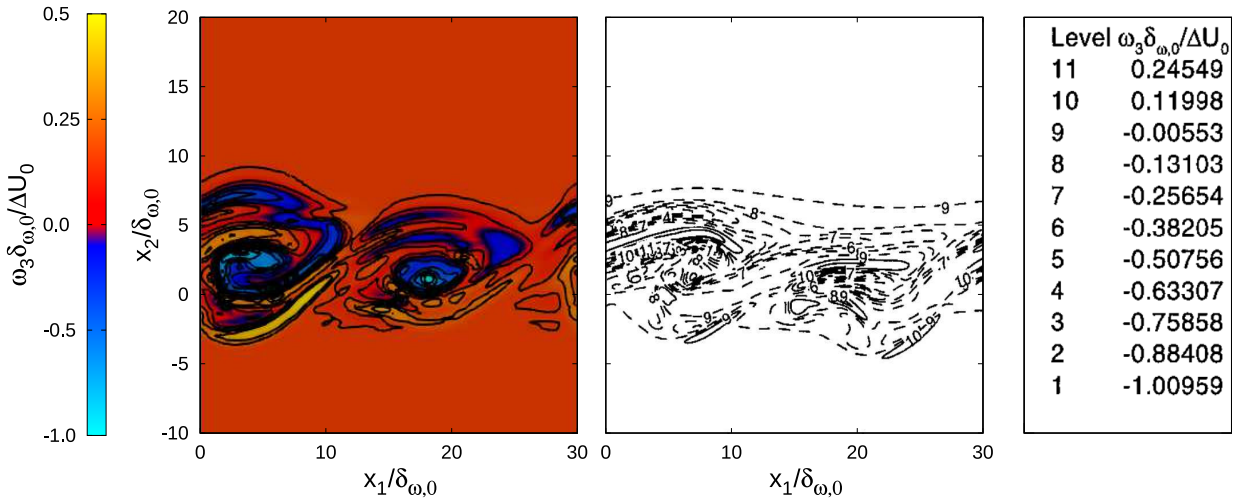

Figure 2. Nondimensional spanwise vorticity at $x_3 = 0.0075$ and $t\Delta U_0/\delta_{\omega,0} = 80$.

It shows some differences in the structures, but the global vortex size and level is in a comparable and acceptable range. This means the global vortex behavior is well predicted by the solver.

Since the major rotation of the vorticity in x_3 direction ω_3 is negative by design, the development of positive ω_3 is an indicator for the development of small turbulent scales. In figure 3 the temporal global positive spanwise vorticity ω_3^+ normalized by $\delta_{\omega,0}$ and the initial velocity difference across the shear layer ΔU_0 is depicted. $\langle\langle\rangle\rangle$ means volume averaging of the quantities in the original simulation domain.

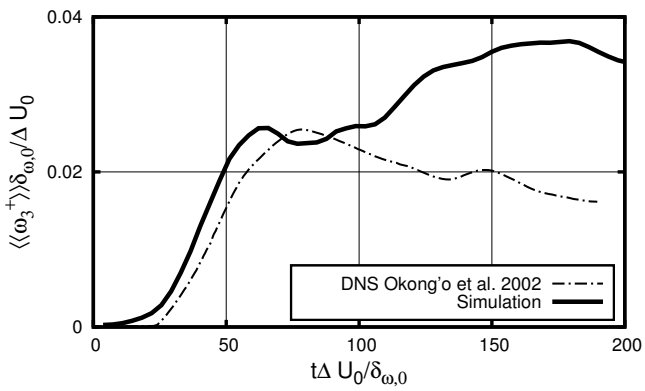

Figure 3. Global positive spanwise vorticity.

In the beginning the development of the positive spanwise vorticity is close to the reference data, but ω_3 is increasing prior to the reference data. After reaching the maximum peak the simulation behavior differs from the DNS data by accumulating more positive spanwise vorticity, than slowly decreasing and reducing those scales.

An additional accessible value is the nondimensional enstrophy $\langle\langle\omega_i\omega_i\rangle\rangle\,(\delta_{\omega,0}/\Delta U_0)^2$, depicted in figure 4. This quantity is an indicator for turbulent tilting and streching mechanisms. In addition to ω_3^+ this is an information for formation processes of small scales.

In this figure a significant stronger accumulation of volume averaged enstrophy is observed. This is pointing to an overprediction of small turbulent scales and in opposition a underestimation of viscous effects.

This work is licensed under a Creative Commons 4.0 International License (CC BY-NC-ND 4.0).

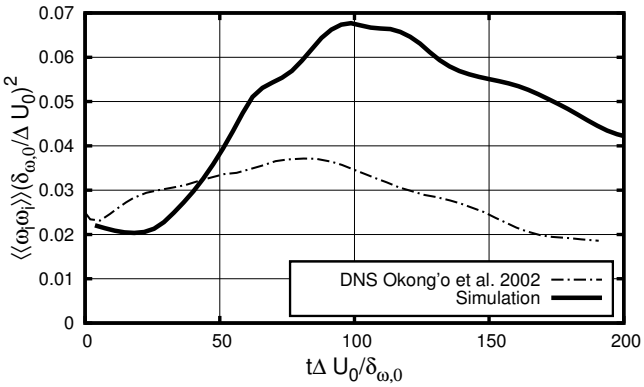

Figure 4. Global positive spanwise enstrophy.

Conclusion

The volume averaged positive global spanwise vorticity is close to the reference data until it reaches the first peak of a maximum in small turbulent scales. Meaning, at that point there are some effects in progress, which tend to overpredict the development of small scales significantly, probably due to the low-Mach approach. At this point an incompressible low-Mach solver is probably not capable of solving such turbulent structures. In the initial state of the simulation the maximum Mach-number is 0.4 which increases during the simulation, leading to greater influence of the growing solution error by unconsidered compressibility effects. Nevertheless the global vortex structures depicted in figure 2 are well predicted. However, the initialization of the test case with a velocity field instead of a vorticity field as in the reference DNS, could also affect the results. Future investigations of the test case regarding low-Mach solver stability and limits will be necessary.

Acknowledgements

The authors gratefully acknowledge the financial support by the DFG (German Research Council) SFB-TRR 75 and the support of the numerical simulations on the Lichtenberg High Performance Computer (HHLR) at the University of Darmstadt. We also gratefully acknowledge the cooperation with Prof. Dr. rer. nat. M. Pfitzner especially M.Sc. C. Traxinger and M.Sc. J. Zips, from the department of thermodynamics at the Universität der Bundeswehr München, regarding the mixture rules implementation.

Nomenclature

A_i	streamwise vorticity coefficients [-]
B_i	spanwise vorticity coefficients [-]
F_{iD}	vorticity coefficients [-]
L_i	domain length [m]
m	mass [kg]
p	pressure [N/m^2]
T	temperature [K]
$\bar{u}_i$	mean velocities [m/s]
x_i	spatial directions [-]
$\delta_{\omega,0}$	initial vorticity thickness [m]
Γ_i	circulation [m^2/s]
λ_i	wavelength [m]
ω_i	vorticity components [$1/s$]
ρ	density [kg/m^3]

References

[1] Chehroudi, B., Cohn, R., Talley, D., 2002, *International Journal of Heat and Fluid Flow* , 23, pp. 554-563.
[2] Mayer, W., and Tamura, H., 1996, *Journal of Propulsion and Power*, 12 (6), pp. 1137-1147.
[3] Roy, A., Joly, C., Segal, C., 2013, *J. Fluid Mech.*, 717, pp. 193-202.
[4] Kawai S., 2019, *J. Fluid Mech.*, 865, pp. 563-601.
[5] Miller, R., N, Harstad, K., Bellan, J., 2001, *J. Fluid Mech.*, 436, pp. 1-39.
[6] Okong'o, N, Harstad, K., Bellan, J., 2002, *AIAA Journal*, 40 (5), pp. 914-926.

This work is licensed under a Creative Commons 4.0 International License (CC BY-NC-ND 4.0).

[7] Peng, D., and Robinson, D., 1976, *Ind. Eng. Chem. Fundamen.*, 15, pp. 59-64.
[8] Ries F., Obando P., Shevchuck I., Janicka J., Sadiki A., 2017, *International Journal of Heat and Fluid Flow*, 66, pp. 172-184.
[9] Ries F., Li Y., Nishad K., Kütemeier D., Mehdizadeh A., Sadiki A., 2019, *11th International Symposium on Turbulence and Shear Flow Phenomena (TSFP11)*
[10] Müller, H., Pfitzner, M., Matheis, J., Hickel, S., 2015, *Journal of Propulsion and Power*, 32 (1), pp. 46-56.
[11] Chung, T., Aljan M., Lee, L., Starling, K., 1988, *Ind. Eng. Chem. Res.*, 27, pp. 671-679.

This work is licensed under a Creative Commons 4.0 International License (CC BY-NC-ND 4.0).